Multiscale Coupling of Sun-Earth Processes
A.T.Y. Lui, Y. Kamide and G. Consolini, editors.

ROLES OF CHAOS, SELF-ORGANIZED CRITICALITY AND PHASE TRANSITIONS IN MAGNETOSPHERIC PHYSICS

M. I. Sitnov
Institute for Research in Electronics and Applied Physics, University of Maryland, College Park, MD 20742, USA

A. Y. Ukhorskiy
Applied Physics Laboratory, The Johns Hopkins University, Laurel, MD 20723-6099, USA

A. S. Sharma
Department of Astronomy, University of Maryland, College Park, MD 20742, USA

R. S. Weigel
LASP, University of Colorado, Boulder, CO 80303, USA

Abstract. Magnetosphere dynamics driven by the solar wind are very complex, involving both coherent responses to the extrernal loading and multiscale features characteristic of critical phenomena. Earlier attempts to explain their complexity in terms of dynamical chaos did not take into account the spatially extended nature of the system and multiscale coupling. A more consistent description can be made using cellular automata models. In particular, the hypothesis of the self-organized critical state of the magnetosphere, which is based on a certain class of cellular automata models, provides a physical basis for the observed power-law spectra of magnetospheric activity. However, this is not enough to explain other features of this activity such as the characteristic scales of storms and substorms and apparent dependence of these phenomena on the solar wind loading. The analysis of correlated sets of solar wind and auroral index data suggest a more general framework for modeling the magnetospheric activity. It reveals in particular both the multiscale processes resembling classical critical phenomena in phase transition physics and regular components of dynamics, which resemble first order phase transitions. Similar to classical critical phenomena, the multiscale properties of substorms depend on the solar wind parameters. Thus, the data-derived picture of substorms differs from the self-organized criticality. However, it is surprisingly consistent with a modern theory of critical phenomena based on cellular-automata with finite driving and dissipation rates, which considers self-organized criticality as a limiting regime of the special type of phase transitions in non-equilibrium systems. The new framework is shown also to provide efficient tools for predicting both global and multiscale features of magnetospheric activity.

1. Introduction: Data-derived Modeling

At first sight, such a complex system as Earth's magnetosphere requires very sophisticated first-principle modeling tools. An example may be global MHD simulations. However, the use of

first-principle models has many limitations. They often require too much computer resources and yet remain imprecise, for instance, in determining the timing of the substorm onset.

Figure 1. Representation of the magnetosphere in a data-derived approach. Input parameters are represented here by the solar wind speed v, southward component of the interplanetary magnetic field B_s, and dynamical pressure P_{dyn}, while the output is represented by the auroral indices AL and AE reflecting the substorm activity, and the disturbance storm-time index D_{st}.

One can propose another approach to complex system modeling. It is a more pragmatic approach without recourse to the tools of classical physics. For instance, although the dynamics of a human body can in principle be described in terms of quantum mechanics and electrodynamics, physicians and sociologists quite seldom use that type of description in their practice. Let us consider instead our system, the magnetosphere, as a black box with some input and output (Figure 1) and let us try to create a model of system's dynamics directly from data, using the techniques of signal processing, nonlinear dynamics and statistics. This is an empirical or *data-derived approach*. It often provides the optimum level of resolution and strongly complements the first-principle models being more robust and efficient in many applications.

2. Linear Filters

The very first look at the input and output time series of substorm data, an example of which is shown in Figure 2, reveals a clear correlation between the solar wind input (inductive electric field parameter vB_s) and the magnetospheric output (AL index). This clear correlation gave rise to the first family of data-derived models of the solar wind-magnetosphere coupling, namely the linear filters [*Burton et al.* 1975, *Iyemori et al.*, 1979; *Clauer et al.*, 1983; *Bargatze et al.*, 1985].

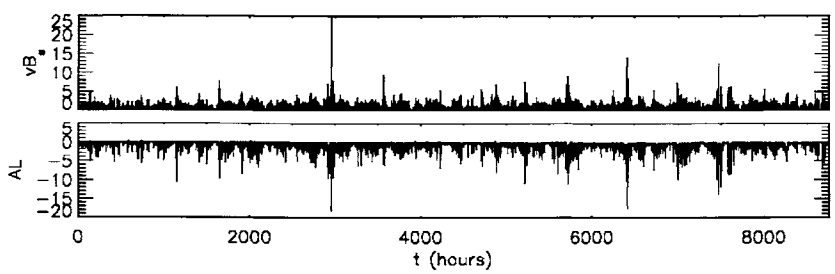

Figure 2. vB_s - AL time series with 1 minute resolution compiled by *Weigel et al.* [2001] for the whole year 1998.

In linear filters the output is supposed to be a linear combination of the input with different time delays

$$O(t) = \int_0^\infty d\tau f(\tau) I(t-\tau). \tag{2.1}$$

If the response is indeed linear, the filter function f will be independent of the activity level. However, already the early studies [*Bargatze et al.*, 1985] revealed the significant dependence of linear filters on the activity level and thus suggested the nonlinearity of the magnetospheric response to the solar wind loading.

3. Dynamical Chaos Hypothesis

Nonlinearity often results in phase divergence, as it takes place, for example, in a nonlinear pendulum. Such a divergence in bounded systems may be a mechanism of dynamical chaos [e.g., *Tabor*, 1989]. The hypothesis that the magnetosphere may be in a regime of dynamical chaos appeared to explain the seeming randomness of the auroral index time series. Note here that most dynamical chaos models deal with autonomous systems, which is not the case for magnetospheric activity represented by the auroral indices, as is clear from Figure 2. However, the closer examination [e.g., *Kamide and Baumjohann*, 1993] reveals that the substorm current system at the ionospheric level, which contributes to the auroral index dynamics, consists of two subsystems, DP1 and DP2. While the DP2 system is actually directly driven by the solar wind input, the DP1 system shows rather autonomous "unloading" behavior.

It was suggested [*Vassiliadis et al.*, 1990; *Roberts*, 1991; *Shan et al.*, 1991a, 1991b; *Pavlos et al.*, 1992, 1994; *Sharma et al.*, 1993] that the complex dynamics of the magnetosphere is *self-organized* and as a result it is controlled by a few effective degrees of freedom, while its complexity arises from the dynamical chaos effects. If that is true than the form of the attractor of the magnetospheric dynamics may be reconstructed using the time delay technique. It can be elucidated by the simple chaotic map model, given by the recurrent relation

$$x_{n+1} = Kx_n \mod 1, \tag{3.1}$$

where *mod1* denotes taking the fractional part of the number Kx_n, and K is a constant number. If K<1, the relation (3.1) describes the sequence, which converges to zero. In contrast, if $K>>1$, then for most initial values x_0, the sequence (3.1) looks quite random as shown in Figure 3a. This type of behavior is also called deterministic chaos because of the deterministic rule (3.1). The rule can be inferred from the series x_n if one plots x_n versus x_{n-1} as shown in Figure 3b

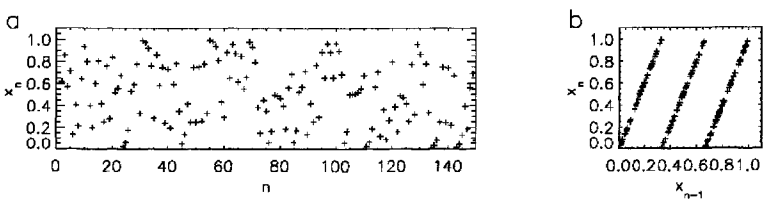

Figure 3. Pseudo-random series x_n generated by the map (3.1) with $x_0 = \sqrt{15}$ and $K=3$ (a), and the reconstruction of the deterministic rule (3.1) using time delays (b).

This simple example has several important implications. First, it shows that the seemingly random dynamics of a nonlinear low-dimensional system can be reconstructed using the *time-delay embedding technique*, that is by plotting the original series in an artificial phase space formed by the original variable and others constructed from the same variable using various time delays. Such an approach was proposed by *Packard et al.* [1980] and *Takens* [1981]. Second, the regular structure of the reconstructed attractor in Figure 3b suggests that the time series x_n as a function of the discrete "time" n can be predicted using local approximation of the attractor. The

corresponding technique of *locally linear filters* was elaborated [e.g., *Casdagli*, 1992] and then applied to forecasting of storms and substorms [*Vassiliadis et al.*, 1995; *Valdivia et al.*, 1996] along with other classes of low-dimensional deterministic models [*Baker et al.*, 1990; *Klimas et al.*, 1992; *Hernandes et al.*, 1993; *Horton and Doxas*, 1998; *Weigel et al.*, 1999]. First estimates of the effective dimension D of the magnetosphere, the so-called correlation dimension [*Grassberger and Procaccia*, 1983], gave very optimistic results with D ranging between 2 and 4 [*Vassiliadis et al.*, 1990; *Roberts*, 1991; *Shan et al.*, 1991]. Moreover, the fact that D was a noninteger number suggested the "strange" character of the attractor [*Lorenz*, 1963], which might explain, in turn, the multiscale features of the substorm structure and dynamics.

4. Self-organized Criticality Models

The dynamical chaos hypothesis was based on one important assumption of low effective dimension of the magnetosphere. However, soon after the first estimates of the correlation dimension of the magnetosphere, *Prichard and Price* [1992] showed that those earlier estimates were caused by the long autocorrelation times of the system rather than by the low-dimensional dynamics. It was shown in particular that the modified correlation integral [*Theiler*, 1986] with excluded pairs of points, which differ in time less than by the autocorrelation time, does not converge for AE index time series. Two possible explanations of that negative result were proposed. There might be strong influence of the solar wind input (most of the dynamical chaos concepts were formulated for autonomous systems) or truly multiscale behavior of the magnetosphere with many excited degrees of freedom. The latter point of view in the form of another paradigm of the so-called *self-organized criticality* (SOC) was strongly motivated by the power-law spectra of the magnetospheric activity. They were first inferred from *AE* index data by *Tsurutani et al.* [1990]. Then *Ohtani et al.* [1995] revealed similar properties of magnetic field fluctuations in the geomagnetotail, consistent with intermittent energy transport phenomena studied by *Angelopoulos et al.* [1994]. The examples of power-law spectra in the form of the burst life time probability distribution [*Freeman et al.*, 2000] and the singular spectrum of solar wind and magnetospheric data [*Sitnov et al.*, 2000] are shown in Figure 4.

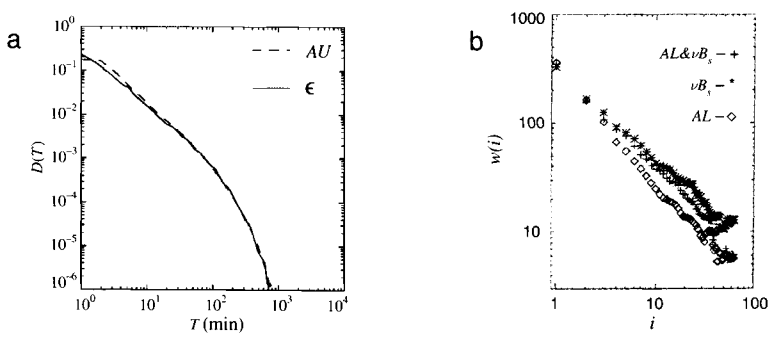

Figure 4. Power-law spectra of solar wind and magnetospheric activity in the forms of (a) life time T probability distribution $D(T)$ of the auroral index AU and Akasofu parameter ε [*Freeman et al.*, 2000] (a burst lifetime, T, is the duration for which the measurement, $AU(t)$ exceeds a given threshold value) and (b) the singular spectrum of AL and vB_s time series as well as their combined set [*Sitnov et al.*, 2000] inferred from first 15 intervals of *Bargatze et al.* [1985] database (for details see equation (5.2) and related discussions in section 5).

Power-law spectra usually indicate that fluctuations of all scales give comparable contributions to dynamics and the smaller scales cannot be simply averaged out. It is interesting to note here that stochastic time series with $1/f^{\alpha}$ power spectra, known as the colored noise, have a finite correlation dimension $D = 2/(\alpha - 1)$ [*Osborne and Provenzale*, 1989] and thus may mimic the dynamical chaos effects in the magnetosphere [*Prichard and Price*, 1992]. To resolve this uncertainty *Theiler* [1991] proposed the method of surrogate data, in which the correlation dimension of the original data is compared with the stochastic time series with the same power spectrum and autocorrelation. The surrogate time series can be formed, for instance, by randomizing the phases of the Fourier transform of the original time series. Using this technique the conclusion on the absence of a converged modified correlation dimension of the magnetosphere inferred from the AE time series has been confirmed [*Price and Prichard*, 1992; *Prichard and Price*, 1992]. Note however that *Roberts* [1991] and *Pavlos* [1992] showed that the data trajectories of AE time series in embedding space may still be drastically different from those of the color noise (for details and further discussions see [*Pavlos et al.*, 1999] and refs. therein, [*Prichard*, 1995] and reviews [*Sharma*, 1995] and [*Klimas et al.*, 1996]).

In 1987 Bak, Tang and Wiesenfeld proposed an elegant model (hereafter BTW), which appeared to explain the ubiquitous nature of power-law fluctuations in different systems. That model as well as its modifications have been later applied by *Consolini* [1997], *Chapman et al.* [1998], and *Uritsky and Pudovkin* [1998] to explain the power-law spectra in the magnetosphere. The original BTW model [*Bak et al.*, 1987] represents a mathematical sandpile, that is a grid of cells, each of which may accumulate some amount of grains Z due to the external loading. When the parameter Z exceeds some threshold value Z_c, which is determined by either the critical slope or energy accumulated in the cell, 4 sand units are transferred to 4 closest cells (the number of cells, 4, is for the specific 2D BTW model):

$$z_{t+1}(x,y) = z_t(x,y); \qquad \mathbf{z} \le \mathbf{z_c}, \tag{4.1}$$

$$z_{t+1}(x \pm 1, y \pm 1) = z_t(x \pm 1, y \pm 1) + 1; \quad z_{t+1}(x,y) = z_t(x,y) - 4, \qquad \mathbf{z} > \mathbf{z_c}, \tag{4.2}$$

Bak et al. [1987] argued that this model reveals the power spectra distributions of avalanches in their size and energy independent of the details of the driving process. To highlight the latter property and distinguish the process from conventional critical phenomena [e.g., *Stanley*, 1971] also known as the second order phase transitions, they called it the self-organized criticality. SOC has been documented in various systems, including rice piles, type II superconductors, droplet formation and a multitude of computer models [e.g., *Jensen*, 1998 and refs. therein].

SOC as a new paradigm for geomagnetic activity has been further tested by *Freeman et al.* [2000], *Consolini and Chang* [2001], *Chapman and Watkins* [2001], and *Watkins et al.* [2001]. In particular, *Consolini and Chang* [2001] discussed a modification of the SOC concept, taking into account the variable solar wind input (the so-called forced self-organized criticality). *Freeman et al.* [2000] and *Chapman and Watkins* [2001] discussed the possibility to separate the autonomous SOC behavior reflected in power-law spectra of auroral indices from its part, possibly related to the DP2 system, which is directly driven by the solar wind. *Watkins et al.* [2001] elucidated that SOC is not an aspect of the global magnetosphere but relevant more locally to the magnetotail. *Takalo et al.* [1999a, 1999b], *Klimas et al.* [2000] and *Uritsky et al.* [2002] studied a class of continuum running avalanche models of the tail current sheet based on a resistive MHD model.

Due largely to the amazing simplicity and seeming universality of the original BTW model, the SOC concept has become very popular in complexity studies. However, it was soon realized that the BTW model is not as ubiquitous as expected and it does not describe in particular the sand dunes themselves. It has been shown [*Nagel*, 1992] that sand behaves in a manner more reminiscent of a first order phase transition than of a second one. Similarly, in the magnetopshere,

in spite of the scale-invariant behavior of some parameters, there are clear signatures of characteristic time scales associated with storms (~ days) and substorms (~ hours). More rigorous results were obtained by *Borovsky et al.* [1993], *Prichard et al.* [1996], and *Smith et al.* [1996], who showed, in particular, that the intensity and inter-substorm interval for one-half of substorms have the probability distribution with a well-defined mean. This apparent contradiction between scale invariance in index spectra on the one hand and the appearance of time and magnitude scales in substorm data on the other hand stimulated *Chapman et al.* [1998] to propose for explanation of the magnetospheric activity an advanced avalanche model elaborated by *Dendy and Helander* [1998]. In contrast to the classical BTW cellular automation, the new model was continuous in height and slope with the threshold condition governed by a probabilistic rule. It demonstrated two types of avalanches, internal that did not reach the edges of the system, and systemwide ones. Internal avalanches reproduced the classical SOC picture with the absence of an intrinsic scale. In contrast, the systemwide discharges had the probability distribution of the time intervals between each discharge and the next with a well-defined mean. Those systemwide avalanches were interpreted by *Chapman et al.* [1998] as substorms.

It is worth noting here that the fundamental physical processes in magnetospheric plasmas underlying their complex dynamical behavior may not allow scale-invariance in the form of avalanches. For instance, in contrast to current disruption phenomena [e.g., *Lui*, 2002 and refs. therein], which indeed resemble avalanches in a ricepile, the processes of magnetic reconnection [e.g., *Birn et al.*, 2001] reveal scale-invariance only near the singular X-line, whereas the minimum size L of a plasmoid formed by reconnection is too large $L \geq\sim 4R_E$ [*Ieda et al.*, 1998] to be utilized in any granular multiscale model of the magnetospheric activity.

Another important feature of magnetospheric dynamics, which distinguishes it from SOC, is its strong dependence on the solar wind input. This dependence is evident from Figure 1 and is confirmed by the successful use of linear and nonlinear filters in forecasting the magnetospheric activity as discussed in more detail in the sections 2 and 3. Moreover, even the multiscale features of this activity are strongly affected by the solar wind input. In particular, such parameters as the fractal dimension [*Uritsky and Pudovkin*, 1998] or κ-exponent in the sign-singular analysis [*Consolini and Lui*, 1999] show clear dependence on the substorm phase, which is controlled in turn by the solar wind loading. Thus, the original 1987 SOC paradigm does not seem to be quite useful for modeling and particularly forecasting of the magnetospheric activity. It introduces however a very promising *probabilistic description* of this activity and highlights its scale-invariant features, which were explicitly demonstrated by *Lui et al.* [2000] and *Uritsky et al.* [2002] on the basis of Polar data. The most important lesson of SOC, according to *Jensen* [1998], is that, in a great variety of systems, it is misleading to neglect the fluctuations.

5. Data-derived Picture of Solar Wind-Magnetosphere Coupling: Analogy with Phase Transitions

Another class of magnetospheric activity models, which reconciles the hypothesis of dynamical chaos and the seemingly alternative SOC interpretation, resulted from the attempts to improve the low-dimensional description of the solar wind-magnetosphere interaction and to elucidate in particular the role of the solar wind driving. In contrast to the previous works based on the assumption that the dynamics of the magnetosphere is autonomous [*Vassiliadis et al.*, 1990; *Roberts*, 1991; *Shan et al.*, 1991b; *Sharma et al.*, 1993], an attempt was made [*Sitnov et al.*, 2000] to construct a low-dimensional input-output relationship, or improve it as compared to its simplest form of linear filters. For that purpose the data were studied in the time-delay space involving both the output of the system (the auroral index AL) and its solar-wind input (the parameter vB_s)

$$\mathbf{X} = \left(\mathbf{O}_t^T, \mathbf{I}_t^T\right) = \left(O_t, ..., O_{t-(M-1)}, I_t, ..., I_{t-(M-1)}\right), \quad I_t = vB_s(t)/\sigma_{vB_s}, \quad O_t = AL(t)/\sigma_{AL}, \tag{5.1}$$

with both input and output parameter being normalized by their standard deviations σ. The resulting expanded time series were additionally sorted using the singular spectrum analysis (SSA) [*Broomhead and King*, 1986] to reveal their linear combinations, which are essential to reproduce the dynamics of the system adequately. In the SSA the matrix X is expanded in a series of projections P_i through the singular value decomposition [e.g., *Press et al.*, 1992]

$$\mathbf{X} = \mathbf{UWV}^T, \quad P_i = (\mathbf{XV})_i, \tag{5.2}$$

where **W** is the diagonal matrix, whose values w_i reflect the significance of projections P_i so that the spectrum w_i resembles the corresponding Fourier and wavelet spectra with the data-derived basis functions [e.g., *Preisendorfer*, 1988].

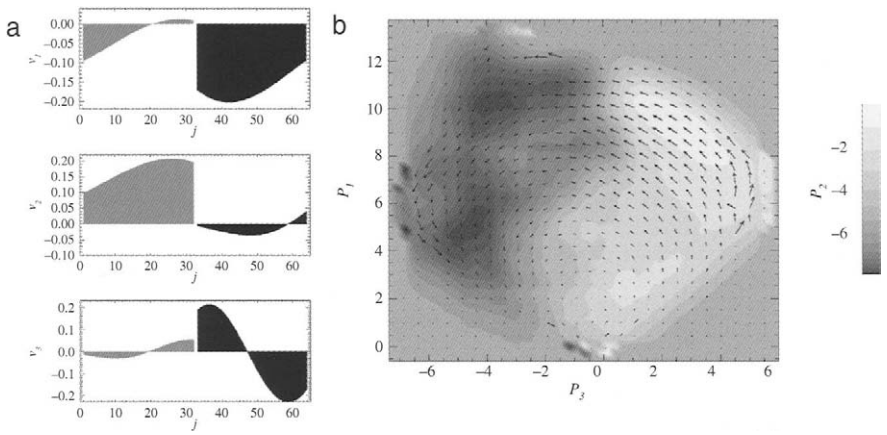

Figure 5. Eigenvectors corresponding to three largest SSA eigenvalues w_i, i=1,2,3 for embedding (5.1) with *M=32* inferred from first 20 intervals of *Bargatze et al.* [1985] database (a) and the 2D manifold of the magnetospheric dynamics in the space of the corresponding projections P_i. The arrows show the data-derived circulation flows of the system $(\dot{P}_1, \dot{P}_3)$.

Sitnov et al. [2000] found that, in contrast to the correlation dimension, and in spite of the fact that the SSA spectrum is a power-law, the more general dimension estimate, the so-called coast-line dimension D_f [e.g., *Abarbanel et al.*, 1993] saturates as a function of the embedded dimension *2M* in the region $D_f \in (2,3)$, and this saturation persists with an increase in the number of the data points for the largest scales. This implies that the magnetosphere trajectory in the embedded input-output phase space lies close to some two-dimensional surface. Subsequent attempts to plot that surface as well as the evolution of the magnetosphere on it gave surprisingly interesting results shown in Figure 5.

The substorm dynamics of the magnetosphere appears in this data-derived picture as a counter-clockwise motion of a point on a two-level surface in the 3D space formed by the papameters P_1, P_2, amd P_3. The corresponding projectors V_1, V_2, and V_3 of the matrix **V** are shown in Figure 5a. Together with the general structure (5.1) of the matrix **X** they demonstrate

that the subspace (P_1, P_2, P_3) is formed by two functions of the input P_1 and P_3 (integrated and differential parameter vB_s, top and bottom panels in Figure 5a, respectively) and a function of the output (integrated AL, middle panel). Figure 5b reveals two interesting features of substorm dynamics. First, the substorm onset (the transition from the upper level to the lower one) is associated with the reduction of the solar wind-magnetosphere coupling (saturation of the input P_1 and transition from positive to negative values of the parameter P_3) as suggested and interpreted in detail by *Lyons et al.* [2003]. Second, the whole surface in Figure 5b resembles the temperature-pressure-density diagram of conventional (non-self-organized) water-steam phase transitions [*Stanley*, 1971] shown in Figure 6a. This diagram has a special *critical point* where density jumps disappear, although jumps or singularities are observed for the second derivatives of the thermodynamic potentials such as the heat capacity (Figure 6b). It is also known [e.g., *Stanley*, 1999; *Kadanoff*, 1999] that near the critical point the fluctuations of the system become multiscale with power-law spectra.

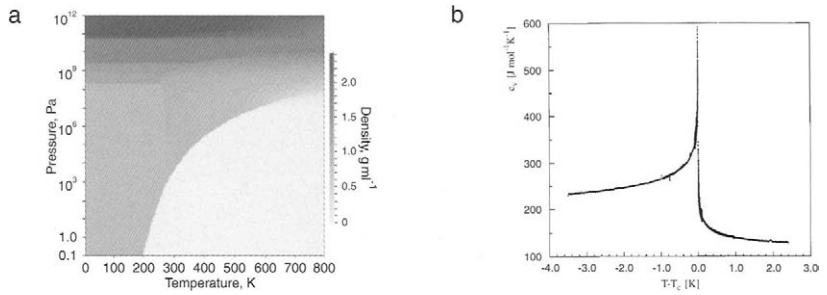

Figure 6. (a) Temperature-pressure-density diagram for water-steam transitions with the critical point (T, P, n)=(647K, 22Mpa, 322 kg/m$_3$) (http://www.lsbu.ac.uk/water/images/den.gif). (b) Specific heat C_V of SF_6 near the critical point [*Haupt and Straub*, 1999].

An important feature of the second order phase transitions, which distinguishes them from other scale-invariant processes and in particular those in the BTW model of SOC, is a series of scale-invariant relationships different from the scale distributions such as AU and AL spectra shown in Figure 4. They relate different parameters of the system such as the temperature fluctuations near the critical point and the corresponding density fluctuations

$$n - n_c \propto \left| T/T_c - 1 \right|^{\beta}, \quad T/T_c - 1 \to 0-, \tag{5.3}$$

Here the parameter β is a critical exponent. *Sitnov et al.* [2001] computed an analog of the critical exponent near the effective critical point $(P_1, P_2, P_3) = (0,0,0)$ in the form of the lower envelope of the derivative dP_2/dt as

$$\min\left(dP_2/dt\right) \propto P_1^{\beta_*}, \tag{5.4}$$

This envelope is shown in Figure 7. It was shown also that within the framework of the simplest mean-field model of phase transition dynamics, the so-called dynamical Ising model [*Zheng and Zhang*, 1998], the exponent β_* is connected to the classical exponent β by the

relation $\beta_* = 3\beta$. Note here that the existence of the multiscale input –output relationship of the type of (5.4) is consistent with the results of *Freeman et al.* [2000] and *Sitnov et al.* [2000] shown

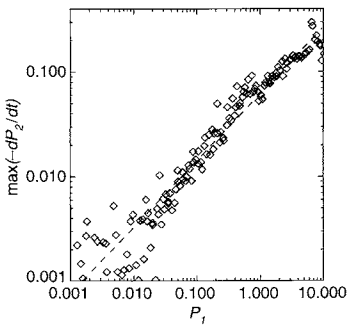

Figure 7. Scale invariant input-output relation of the type of (5.3) with $\beta_* \approx 0.64$ inferred from the SSA analysis of substorm dynamics [*Sitnov et al.*, 2001].

in Figure 4, which reveal close resemblance between solar wind and magnetospheric fluctuation spectra. Although the results of *Freeman et al.* [2000] and similar results by *Hnat et al.* [2002] reveal nearly same spectra of solar wind and auroral indices suggesting that the magnetosphere works as an exhaustive pipe for solar wind and the input-output exponent β should be simple rational number, the results of *Sitnov et al.* [2000] (Figure 4b) as well as the extended analysis of *Hnat et al.* [2002] performed in [*Hnat et al.*, 2003] reveal quite considerable difference between the input and output spectra.

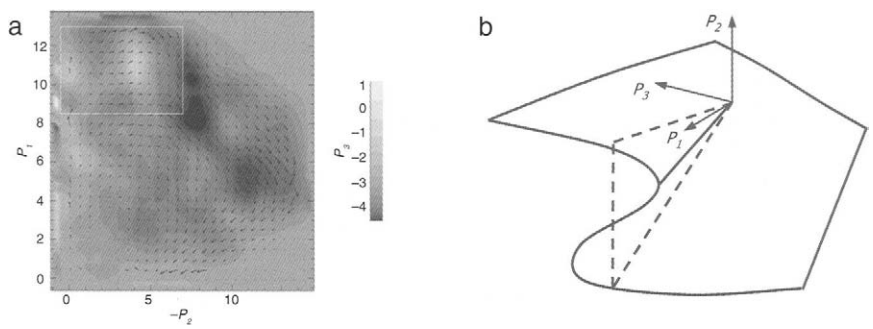

Figure 8. (a) Hysteresis phenomenon (white rectangle) inferred from the SSA analysis of substorm data [*Sitnov et al.*, 2001]. (b) Interpretation of Figure 7a as a phase separation surface of nonequilibrium phase transitions; dashed lines show its analog in the equilibrium case similar to Figure 5a.

The dynamical and non-equilibrium nature of magnetospheric phase transitions during substorms is reflected by the *hysteresis* phenomena, when the system may be in two or more different states under the same quasi-static conditions such as, for instance, its temperature and

pressure. Then the analog of the temperature-pressure-density diagram differs from the equilibrium one shown in Figure 6a and resembles more the one shown in Figure 8b. The original projection of the substorm data shown in Figure 5b cannot reveal hysteresis as the corresponding intervals in data would be folded. In fact, those intervals were removed from the main data set to reveal the two-level surface; however, we show below that the analog of Figure 5b can be obtained without that rather artificial procedure. Another projection shown in Figure 8a reveals the hysteresis phenomena in substorm dynamics.

Hysteresis is closely related to the *metastability* property of the system, because one of many states available at given parameters of the system is often metastable and becomes unstable in presence of fluctuations. The fact that the magnetosphere during substorms behaves as a metastable system is reflected in many models of the substorm onset in the form of the corresponding plasma instabilities and catastrophes [*Goertz and Smith*, 1989; *Sitnov et al.*, 1997; *Hurricane et al.*, 1998; *Birn et al.*, 2004].

The apparent controversy between the data-derived picture of the magnetospheric dynamics described above and the classical SOC model [*Bak et al.*, 1987] has been resolved recently within the framework of the SOC theory itself. *Vespignani and Zapperi* [1998] noted that the BTW model contains a condition, which is quite unusual for real open systems. Specifically, each new grain of sand is added to the pile after the completion of all avalanches induced by previous grains. This makes the loading rate the smallest parameter in the model. According to *Vespignani and Zapperi* [1998], elimination of the aforementioned condition almost restores the conventional picture of phase transitions for both classical SOC models, sandpile and forest fire model. There exists, in particular, an analog of the temperature-pressure-density diagram similar to Figure 5b (Fig.1 in [*Vespignani and Zapperi*, 1998]) as well as the input-output multiscale relationship similar to (5.3) and (5.4) and Figure 7 (Figs.2 and 3 in [*Vespignani and Zapperi*, 1998]). According to *Vespignani and Zapperi* [1998], the genuine SOC regime arises only in the limit when both driving and dissipation rates tend to zero. On the other hand, the behavior of cellular automata beyond the SOC regime still has an important feature, which distinguishes them from conventional water-steam transitions. Having driving and dissipation rates as the control parameters instead of the state parameters such as the pressure or temperature, these transitions turn out to be inherently non-equilibrium.

These results have been further substantiated by *Consolini and De Michelis* [2001], who studied a revised forest-fire model driven by a 1D coupled map, which shows on-off intermittency with quiet and turbulent periods and thus is able to mimic the important features of the solar wind driving of the Earth's magnetosphere. They report in particular the criticality, which is "forced" rather than "self-organized" and is very similar to ordinary critical phenomena with first and second order phase transitions. A transition from the avalanche regime characteristic of SOC to another, "continuous flow" regime was also reported by *Corral and Paczuski* [1999] for the so-called "Oslo" model, which is widely used in SOC studies. In contrast to the avalanche regime, where the width of the active zone diverges with system size, in the continuous flow regime the active zone width is independent of the system size. The transition to the continuous flow regime occurs when the time between grain additions becomes comparable with the mean avalanche time. A seemingly different result on the robustness of the SOC behavior under strong driving conditions has been reported by *Watkins et al.* [1999]. However, *Watkins et al.* [1999] used in their analysis a modified sandpile model [*Dendy and Helander*, 1998; *Chapman et al.*, 1998], in which the probability distribution already contains both the SOC-like power-law constituent and a non-SOC part with a characteristic scale.

6. Phase Transition Analogy Applications: New Generation of Forecasting Tools

The phase transition analogy revealed in the analysis of the correlated solar wind-magnetosphere data made several important contributions to our understanding of modeling solar

wind-magnetosphere interaction. First, it showed that global coherent and multiscale phenomena may co-exist like first- and second order transitions do in the water-steam system. Second, it revealed the importance of averaging in the reconstructed phase space necessary to reveal the "mean-field" dynamical features (figures 5b and 8a). Third, it confirmed that the mutiscale features of the magnetospheric dynamics may depend on the solar wind conditions. Therefore, the probabilistic description of those multiscale features must have the form of *conditional* probabilities. The utilization of these new concepts have resulted in creating a new generation of tools to model and forecast the magnetospheric activity.

6.1 Mean-field dimension

In the mean-field approach the dynamics of the system is approximated by the motion of the center of mass of its *NN* nearest neighbors in the embedded and SSA-ordered phase space

$$\mathbf{x}_t^{cm} = \sum_{i=1}^{NN} \mathbf{x}_i, \quad \mathbf{x}_t = \left(I_t,...,I_{t-(M-1)},O_t,...,O_{t-(M-1)}\right)\left(\mathbf{v}_1,...\mathbf{v}_D\right), \quad \left\|\mathbf{x}_i - \mathbf{x}_t\right\| < \varepsilon\left(NN\right), \tag{6.1}$$

where $\mathbf{v}_i$, $i=1,...D$, is the ith column of the orthogonal projection matrix V in the singular value decomposition (5.2), and $\varepsilon(NN)$ is the minimum radius of an n-dimensional sphere containing the nearest neighbors. In particular, the next step in time is given by the formula

$$O_{t+1}^{mf} = F\left(\mathbf{x}_t^{cm}\right) = \left\langle O_{k+1} \right\rangle, \quad \mathbf{x}_k \in NN, \tag{6.2}$$

The minimum embedding dimension D in these equations is determined by the condition of a regular behavior of the function F. The point is that the averaging procedure in multiscale systems often becomes incorrect as it takes place, for instance, in case of the phase transitions near the critical point [*Kadanoff*, 1999]. On the other hand, the theory of critical phenomena [e. g., *Kadanoff*, 1999 and refs. therein] as well as the dynamical system theory [e.g., *Casdagli*, 1992] suggest that the mean-field description based on the averaging procedure may be correct if the dimension is high enough. This is the dimension we search for. In particular, as suggested by *Ukhorskiy et al.* [2003], given the specific number of *NN* and accuracy ε_F we calculate the minimum dimension $D=D_t$, for which the following condition holds

$$\left|O_{t+1}^{mf} - \widetilde{O}_{t+1}^{mf}\right| < \varepsilon_F, \tag{6.3}$$

where $\widetilde{O}_{t+1}^{mf}$ differs from O_{t+1}^{mf} given by (6.2) in that the set of the nearest neighbors of $\mathbf{x}_t$ includes now the point $\mathbf{x}_t$ itself. Then the optimum *mean-field dimension* D_{mf} of the system for a given pair (NN, ε_F) is found as a cut-off of the probability distribution function $P(D_t)$. This definition of dimension ensures the regular character of the forecasting process (6.2). Its dependence on the averaging level *NN* is also quite natural as in practice the dimension does depend on the region of scales considered (one can propose as an example a seashell, which is 1D at scales more them 10cm, 2D at 1 cm scale and 3D at smaller scales). The effective dimension $D_{mf}=3$, consistent with the SSA images in Figures 5b and 8a, has been found for $NN=300$ [*Ukhorskiy et al.*, 2003]. Moreover, the new probabilistic approach allows us to provide the analog of Figure 5b without removing hysteresis intervals from the original data set. The hysteresis phenomena responsible for the folding of the surface shown in Figure 8a make the

distribution of trajectory points $P(P_2)$ double peaked. However, one of two peaks of that distribution is usually larger than the other, and the former peak determines the value of the parameters P_2 for the corresponding equilibrium system (for details see, for instance [*Gilmore*, 1993]). The maximum probability plots $\tilde{P}_2(P_1, P_3)$, $P(\tilde{P}_2) = \max P(P_2)_{|P_1,P_2}$ for two different data sets [*Bargatze et al.*, 1985] and [*Weigel et al.*, 2001] are shown in Figure 9. Note that the former data set includes only non-storm substorms of different averaged levels of activity, while the latter one represents just one year record of *AL* and vB_s parameters including both storm and non-storm substorms. The amazing similarity of plots in Figure 9 with conventional temperature-pressure-density diagram of water-steam transitions (Figure 6) strongly supports the hypothesis of the phase transition-like behavior of the magnetospheric index AL during substorms.

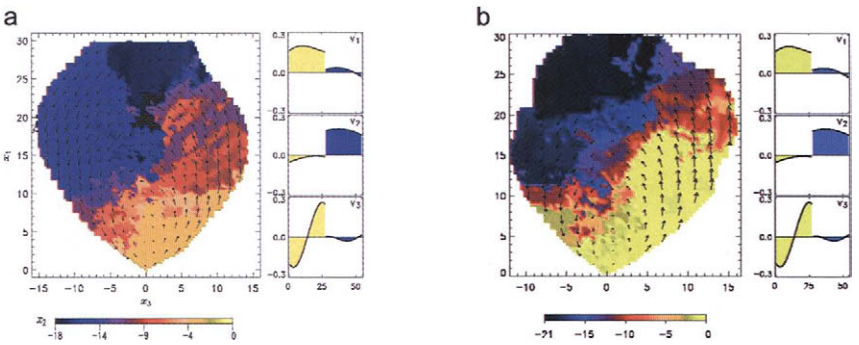

Figure 9. Substrom dynamics of the magnetosphere inferred from the singular spectrum analysis of *AL*-vB_s data for *Bargatze et al.* [1985] (a) and *Weigel et al.* [2001] (b) data sets. Different colors code maxima of the conditional probability distribution $P(x_2|x_1,x_3)$. Structure of the SSA eigenvectors v_n, which determine the relation of the variables x_n, to the original time series *AL* and vB_s through (6.1), are shown in yellow-blue panels.

6.2 Conditional probability approach to forecasting of substorm activity

Owing to equation (6.2) the mean-field description provides the forecasting algorithm similar to that of nonlinear filters, which is superior to the linear filter approach. Moreover, in contrast to nonlinear filters and similar to linear ones, the optimization of this nonlinear algorithm involves only one global parameter D_{mf} and therefore significantly improves deterministic predictions. This type of prediction becomes possible in spite of the power-law spectra of the output fluctuations as the system is strongly driven by the solar wind input. In particular, *Ukhorskiy et al.* [2004a] have shown that the *conditional probability* distributions $P(O|I)$, which constitute the almost power-law marginal distribution $P(O)$ in case of the solar wind-magnetosphere system described by *AL* and vB_s are much more localized and non-power-law. This fact not only justifies the mean-field deterministic forecasting algorithm (6.2) but allows to further improve predictions by supplying each specific value of the deterministic forecast O_{t+1} at given time $t+1$ with the conditional probability bar $P(O_{t+1}|I)$

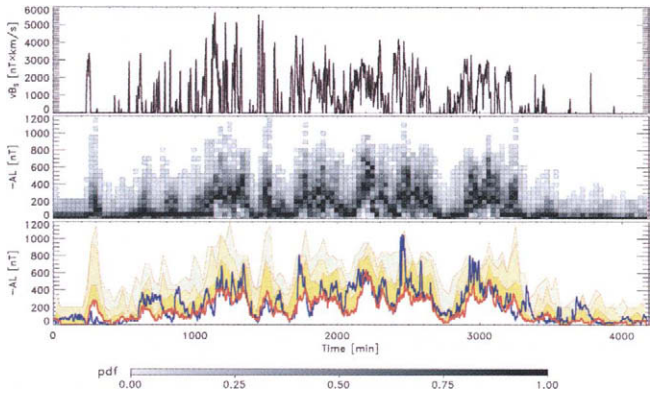

Figure 10. Mean-field and conditional probability (gray and color shading) predictions of AL index (blue) using the solar wind data input (top panel) for the 27th interval of *Bargatze et al.* [1985] database. Middle panel shows the probability $P(O_{t+1}|\mathbf{x}_t)$ of AL with the optimum choice $(D_{mf}, NN)=(5, 50)$. Bottom panel shows the mean-field forecast O_{t+1}^{mf} (red) and the conditional probability $P\left(O_{t+1} > O_{t+1}^{mf} \mid \mathbf{x}_t\right)$ of deviations from O_{t+1}^{mf} with $P \le 0.7$ (dark yellow), 0.9 (yellow) and 1 (light yellow).

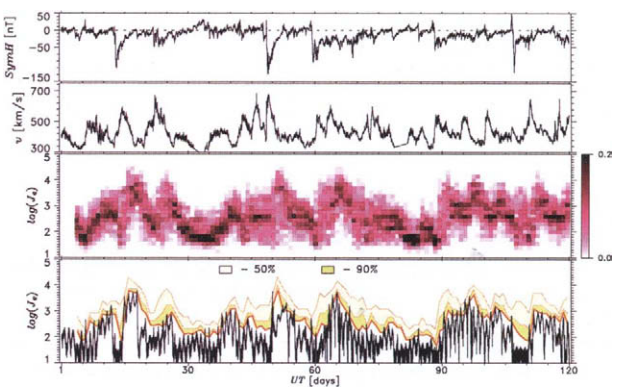

Figure 11. One-day predictions of relativistic electron intensity at geosynchronous orbit ($M=3$, $NN=300$) for a part of of 1999. Inputs: the *SymH* index (top panel) and the solar wind velocity (upper middle panel). Outputs: the conditional probabilities $P\left(O_{t+1} \mid x_t\right)$ (lower middle panel), predicted $\log\left(J_e^{\max}\right)$ (red, bottom panel), contours of probability $P\left(\delta_{t+1} \mid x_t\right)$ (yellow shading, bottom panel) for the actual $\log\left(J_e\right)$ (black, bottom panel) to exceed the predicted $\log\left(J_e^{\max}\right)$ under the given solar wind and magnetospheric conditions.

$$P(O_{t+1} \mid \mathbf{x}_t) \simeq P(O_{k+1}), \quad \mathbf{x}_k \in NN, \tag{6.4}$$

showing the predicted distribution of deviations from that deterministic value O_{t+1} due to the multiscale properties of the system.

An example of such predictions for *Bargatze et al.* [1985] data set is shown in Figure 10. It shows in particular that the mean-field model (6.2) forecast (bottom panel, red curve) is quite efficient in reproducing the average dynamics of *AL*. In contrast to earlier locally linear filter techniques [*Vassiliadis et al.*, 1995; *Valdivia et al.*, 1996], the new method does not require any tuning of the filter parameters, as demonstrated by *Ukhorskiy et al.* [2002], as long as the mean-field dimension is D_{mf} determined using the procedure described in the previous subsection. The complementary conditional probability forecasts are given in Figure 10 in two forms. First, the middle panel shows the probability $P(O_{t+1}|x_t)$ of *AL* with the optimum choice $(D_{mf}, NN)=(5, 50)$. The bottom panel gives the conditional probability $P\left(O_{t+1} > O_{t+1}^{mf} \mid \mathbf{x}_t\right)$ of deviations from the mean-field forecast O_{t+1}^{mf}. The probability distributions are computed at each time step using only those events that correspond to AL values greater than the mean-field model output. In particular, the 100% contour includes all deviations from the meanfield prediction, including the sharpest peaks.

6.3 Conditional probability forecasting of radiation belt electron fluxes

The unified data-derived description based on the combination of mean-field dynamical model and conditional probability approach provides an efficient technique for modeling and forecasting various magnetospheric time series. *Ukhorskiy et al.* [2004b] used this technique for one-day predictions of the MeV electron fluxes at geosynchronous orbit. The parameters of the model were derived from the correlated database of solar wind parameters, geomagnetic indices, and daily maxima of relativistic (> 2 MeV) electron flux observed by GOES 7 and 8 satellites during years 1995 through 2000. The logarithm of the flux daily maxima was taken as the output of the model, i.e $O_t = \log\left(J_e^{\max}\right)$. The model was driven with daily maxima of the input parameters

$$\left(I_t^{(1)}, \ldots I_t^{(5)}\right) = \max\left(v, -SymH, vB_s, P_{dyn}, AsyH\right), \tag{6.5}$$

where *SymH* and *AsyH* are longitudinally symmetric and asymmetric mid-latitude geomagnetic indices, respectively, with the former one being often considered as a high-resolution analog of the *Dst* index.

The small-scale dynamics of electrons in the outer radiation belt have a multiscale nature due to stochastic interactions with various wave fields. In a first principle approach averaging over these small scales yields a set of diffusion equations that govern the large-scale dynamics of the electron fluxes. To derive the global dynamical constituent *Ukhorskiy et al.* [2004b] used the mean-field dynamical approach based on the ensemble averaging of similar states in the reconstructed phase space of mean-field dimension. In particular, it was shown that the mean-field model yields the average prediction efficiency of 0.77, which exceeds the predictability of diffusion-based models [*Li et al.*, 2001] by about 0.2.

To describe the constituent of the MeV electron flux time series not captured by the deterministic model the conditional probability approach was used. The conditional probabilities were calculated using (6.4). Since the mean-field model often underestimates the fluxes,

$P(O_{t+1} \mid \mathbf{x}_t)$ was used to evaluate the probability $P(\delta_{t+1} \mid \mathbf{x}_t)$ of the observed value of the flux O_{t+1} to exceed its predicted value $\widehat{O}_{t+1}$, where $\delta_t = O_t - \widehat{O}_t$, for $O_t > \widehat{O}_t$, and *0* for $O_t \le \widehat{O}_t$.

At each time step the output of the deterministic model was supplemented with the corresponding probability contours δ_t^C

$$\int_0^{\delta_t^C} P(\delta \mid \mathbf{x}_{t-1}) d\delta = C, \tag{6.6}$$

which were used in risk analysis forecasting. For example, *C=1* corresponds the highest possible value of the flux, while *C=0.7* corresponds to the flux level which is not exceeded in 70% of the cases.

An example of one-day prediction of the combined model given by the mean-field and conditional probability descriptions together is shown in Figure 11. Taking into account the relatively limited amount of data, the calculation of the mean-field dimension was replaced in this case by the straightforward optimization of the mean-field evolution equation (6.2) over the parameters M and *NN*. In particular, the optimal set (*M=3, NN=300*) used to Figure 11 gives the highest Prediction Efficiency *PE=1-MSE/VAR*, where *MSE* is the mean squared error and *VAR* is the variance of the observed time series.

The most relevant input parameters *v* and *SymH* are shown in top panels of the figure. The time series of $\log(J_e)$ are shown in black in the bottom panel and the one-day predictions of $\log(J_e^{\max})$ are shown in red. The large daily variations of $\log(J_e^{\max})$ are caused by the satellite rotation around the Earth. The time series of predicted $\log(J_e^{\max})$ has one-day time scale and provides an upper envelope for the observed variations of the flux. The conditional probabilities of $\log(J_e^{\max})$ calculated at each time step are shown in the third panel and these are used to calculate the probability contours shown in different shades of yellow above the predicted value of $\log(J_e^{\max})$ in the bottom panel. This way the model yields risks of deviations from deterministic predictions as a function of the average solar wind and magnetosphere conditions.

To validate the probabilistic approach one must answer the following question. Being calculated using in-sample statistics, how does $P(\delta_t \mid x_{t-1})$ perform out-of-sample? In other words, by the construction δ_t^C probability contours embrace *C·100%* of in-sample events, will it still hold for out-of-sample predictions? To answer the first question we calculate the following average of (6.6) over all $\mathbf{x}_{t-1}$

$$C = \sum_t P(\mathbf{x}_{t-1}) \int_0^{\delta_t^C} P(\delta \mid \mathbf{x}_{t-1}) d\delta, \tag{6.7}$$

for out-of sample predictions. Note that for in-sample predictions (6.7) becomes an identity by virtue of the definition (6.6). On the other hand, using the definition of the conditional probability, the right hand side of (6.7) can be re-written in the form, which does not contain the unknown function $P(\mathbf{x}_{t-1})$

$$\sum_t P(\mathbf{x}_{t-1}) \int_0^{\delta_t^C} P(\delta \mid \mathbf{x}_{t-1}) d\delta = \int_0^{\delta} P(\delta') d\delta', \tag{6.8}$$

where $\delta' = \delta / \delta_t^C$.

The integrals in the right hand side of (6.8) calculated for out-of-sample predictions of log fluxes for years 1995-2000, are listed in Table 1. The average error is only *0.03*, which means that the in-sample training set provides the sufficient coverage of the dynamic range of the flux and therefore can be used for out-of-sample probabilistic predictions. There are two major sources of the observed uncertainty. First, the events lying outside of the dynamic range of the training set (i.e. most extreme events like the Bastille day 2000 storm), cannot be predicted based on this training set. This explains the fact that *C=1* contour does not embrace 100% of events. Second, due to the coarse partitioning of the flux range used in the calculations the contours corresponding to different values of *C* can coincide at some places, which explains why a given probability contour generally embraces a slightly higher number of events.

Table 1. Integrals (6.8) calculated for out-of-sample predictions of log fluxes for years 1995-2000

C	0.50	0.60	0.70	0.80	0.90	1.0
$\int_0^1 P(\delta')d\delta'$	0.55	0.64	0.73	0.83	0.91	0.97

A more conventional way of estimating the probability contours is based on the marginal probability density function $P(\delta_t)$ calculated with all events in the training set. The resultant contours δ_t^C do not depend on any control parameters and therefore are fixed in time $\delta_t^C \to \delta^C$. The discrepancy between the two approaches can be quantified in terms of the standard deviation $\sigma_C^2 = (1/N)\sum_{t=1}^{N}\left(\delta_t^C / \delta^C - 1\right)^2$, which also shows the variability of the conditional probability functions. The average σ_C calculated for 50-100% contours for years 1995-2000 is as high as 0.5. This means that the shape of conditional probability function strongly depends on the solar wind and magnetospheric conditions and that the probability contours derived from the marginal probability density function in most cases strongly underestimate or overestimate the risks in the system.

7. Conclusion

We have reviewed three types of models of geomagnetic activity, based on the concepts of dynamical chaos, self-organized criticality and nonequilibrium phase transition physics. These concepts are shown to provide important new techniques improving the simplest approach to modeling solar wind-magnetosphere interactions based on linear filters, including (I) time delay embedding, (II) averaging over the nearest neighbors and (III) conditional probability approach. The resulting model of the magnetosphere as a dynamical system reveals interesting new features of substorm dynamics such as an analog of the phase transition diagram, hysteresis, and input-output multiscale relationships. Importantly, these features are consistent with the generalized SOC theory, which treats the BTW regime as a limiting case of the specific class of nonequilibrium phase transitions. This also results in a new generation of forecasting tools with deterministic predictions of the global component of magnetospheric dynamics and probabilistic predictions of its multi-scale features.

Acknowledgements

The research was supported by NSF grants ATM-0119196 and 0318629.

References

Abarbanel, H. D., R. Brown, J. J. Sidorovich, and T. S. Tsimring, The analysis of observed chaotic data in physical systems, *Rev. Mod. Phys., 65*, 1331, 1993.

Angelopoulos, V., C. F. Kennel, F. V. Coroniti, R. Pellat, M. G. Kivelson, R. J. Walker, C. T. Russel, W. Baumjohann, W. C. Feldman, and J. T. Gosling, Statistical characteristics of bursty bulk flow events, *J. Geophys. Res., 99,* 21257, 1994.

Bak, P., C. Tang, and K. Wiesenfeld, Self-organized criticality: An explanation of 1/f noise, *Phys. Rev. Lett., 59,* 381, 1987.

Baker, D. N., A. J. Klimas, R. L. McPherron, and J. Buchner, The evolution from weak to strong geomagnetic activity: An interpretation in terms of deterministic chaos, *Geophys. Res. Lett., 17,* 41, 1990.

Bargatze, L. F., D. N. Baker, R. L. McPherron, and E. W. Hones Jr., Magnetospheric impulse response for many levels of geomagnetic activity, *J. Geophys. Res., 90*(A7), 6387-6394, 1985.

Birn, J., J. F. Drake, M. A. Shay, B. N. Rogers, R. E. Denton, M. Hesse, M. Kuznetsova, Z. W. Ma, A. Bhattacharjee, A. Otto, and P. L. Pritchett, Geospace Environmental Modeling (GEM) Magnetic Reconnection Challenge, *J. Geophys. Res., 106,* 3715, 2001.

Birn, J., J. C. Dorelli, M. Hesse, K., Schindler, Thin current sheets and loss of equilibrium: Three-dimensional theory and simulations, *J. Geophys. Res., 109,* A02215, doi:10.1029/2003JA010275, 2004.

Borovsky, J. E., R. J. Nemzek, and R. D. Balian, The occurrence rate of magnetospheric-substorm onsets: Random and periodic substorms, *J. Geophys. Res., 98,* 3807 1993.

Broomhead, D. S., and G. P. King, Extracting qualitative dynamics from experimental data, *Physica D, 20*, 217, 1986.

Burton, R. K., R. L. McPherron, and C. T. Russell, An emphirical relationship between interplanetary conditions and Dst, *J. Geophys. Res., 80*, 4204, 1975.

Casdagli, M., A dynamical approach to modeling input-output systems, in *Nonlinear Modeling and Forecasting*, Casdagli, M., and S. Eubank, editors, p.265, Addison-Wesley, 1992.

Chapman, S., and N. Watkins, Avalanching and self-organized criticality, a paradigm for geomagnetic activity? *Space Sci. Rev., 95*, 293, 2001.

Chapman, S. C., N. W. Watkins, R. O. Dendy, P. Helander, and G. Rowlands, A simple avalanche model as an analogue for magnetospheric activity, *Geophys. Res. Lett., 25*, 2397, 1998.

Clauer, C. R., R. L. McPherron, and C. Searls, Solar wind control of the low-latitude asymmetric magnetic disturbance field, *J. Geophys. Res., 88*, 2123, 1983.

Consolini, G., Sandpile cellular automata and magnetospheric dynamics, in *Proc. Vol. 58, "Cosmic Physics in the Year 2000"*, edited by S. Aiello, N. Iucci, G. Sironi, A. Traves, and U. Villante, SIF Bologna, Italy, 1997.

Consolini, G., and T. S. Chang, Magnetic field topology and criticality in geotail dynamics: Relevance to substorm phenomena, *Space Sci. Rev., 95*, 309, 2001.

Consolini, G., and P. De Michelis, A revised forest-fire cellular automation for the nonlinear dynamics of the Earth's magnetotail, *J. Atmos. Solar Terr. Phys., 63*, 1371, 2001.

Consolini, G., and A. T. Y. Lui, Sign-singular analysis of current disruption, *Geophys. Res. Lett., 26*, 1673, 1999.

Corral, A., and M. Paczuski, Avalanche merging and continuous flow in a sandpile model, *Phys. Rev. Lett., 83*, 572, 1999.

Dendy, R. O. and P. Helander, On the appearance and non-appearance of self-organised criticality in sandpiles, *Phys. Rev. E, 57*, 3641, 1998.

Freeman, M. P., N. W. Watkins, and D. J. Riley, Evidence for a solar wind origin of the power law burst lifetime distribution of the AE index, *Geophys. Res. Lett., 27*, 1087, 2000.

Gilmore, R., *Catastrophe Theory for Scientists and Engineers*, Dover, Mineola, New York, 1993.
Goertz, C. K., and R. A. Smith, The thermal catastrophe model of substorms, *J. Geophys. Res., 94*, 6581, 1989.
Grassberger, P. and I. Procaccia, Measuring the strangeness of strange attractors, *Physica D, 9*, 189, 1983.
Haupt, A., and J. Straub, Evaluation of the isochoric heat capacity measurements at the critical isochore of SF_6 performed during the German Spacelab Mission D-2, *Phys. Rev. E,* , 1795, 1999.
Hernandes, J. V., T. Tajima, and W. Horton, Neutral net forecasting for geomagnetic activity, *Geophys. Res. Lett., 20*, 2707, 1993.
Hnat, B., S. C. Chapman, G. Rowlands, N. W. Watkins, M. P. Freeman, Scaling in solar wind ε and the AE, AL and AU indices as seen by WIND, *Geophys. Res. Lett., 29(10)*, 1446, doi:10.1029/2001GL014597, 2002.
Hnat, B., S. C. Chapman, G. Rowlands, N. W. Watkins, M. P. Freeman, Scaling in long term data sets of geomagnetic indices and solar wind ε as seen by WIND spacecraft, *Geophys. Res. Lett., 30(22)*, 2174, doi:10.1029/2003GL018209, 2003.
Horton, W., and I. Doxas, A low-dimensional dynamical model for the solar wind driven geotail-ionosphere system, *J. Geophys. Res., 103*, 4561, 1998.
Hurricane, O. A., B. H. Fong, S. C. Cowley, F. V. Coroniti, C. F. Kennel, and R. Pellat, Substorm detonation – the unification of substorm trigger mechanisms, in *Substorms-4: International Conference on Substorms-4, Lake Hamana, Japan, March 9-13, 1998*, edited by S. Kokubun and Y. Kamide, p.373,, Terra Sci., Tokyo, 1998.
Ieda, A., S. Machida, T. Mukai, Y. Saito, T. Yamamoto, A. Nishida, T. Terasawa, S. Kokubun, Statistical analysis of the plasmoid evolution with Geotail observations, *J. Geophys. Res., 103*, 4453, 1998.
Iyemori, T., H. Maeda, and T. Kamei, Impulse response of geomagnetic indices to interplanetary magnetic field, *J. Geomagn. Geoelectr, 6*, 577, 1979.
Jensen, H. J., *Self-Organized Criticality: Emergent Complex Behavior in Physical and Biological Systems*, Cambridge Univ. Press, Cambridge, 1998.
Kadanoff, L. P., *Statistical physics: statics, dynamics and renormalization*, World Scientific Publishing Co. Pte. Ltd, Singapore, 1999.
Kamide, Y., and W. Baumjohann, *Magnetosphere-Ionosphere Coupling*, Springer-Verlag, Berlin Heidelberg, 1993.
Klimas, A. J., D. N. Baker, D. A. Roberts, D. H. Fairfield, and J. Buchner, A nonlinear dynamical analogue model of geomagnetic activity, *J. Geophys. Res., 97*, 12,253, 1992.
Klimas, A. J., D. Vassiliadis, B. N. Baker, and D. A. Roberts, The organized nonlinear dynamics of the magnetosphere, *J. Geophys. Res., 101*, 13,089, 1996.
Klimas, A. J., J. A. Valdivia, D. Vassiliadis, D. N. Baker, M. Hesse, and J. Takalo, The role of self-organized criticality in the substorm phenomenon and its relation to localized reconnection in the magnetospheric plasma sheet, *J. Geophys. Res., 105*, 18,765, 2000.
Li, X., M. Temerin, D. N. Baker, G. D. Reeves, and D. Larson, Quantitative prediction of radiation belt electrons at geostationary orbit based on solar wind measurements, *Geophys. Res. Lett., 28*, 1887, 2001.
Lorenz, E. N., Determining nonperiodic flow, *J. Atmos. Sci., 20*, 130, 1963.
Lui, A. T. Y., Multiscale phenomena in the near-Earth magnetosphere, *J. Atmos. Solar Terr. Phys., 64*, 125, 2002.
Lui, A. T. Y., S. C. Chapman, K. Liou, P. T. Newell, C. I. Meng, M. Brittnacher, G. K. Parks, Is the dynamic magnetosphere an avalanching system?, *Geophys. Res. Lett., 27*, 911, 2000.
Lyons, L. R., S. Liu, J. M. Ruohoniemi, S. I. Solovyev, J. C. Samson, Observations of dayside convection reduction leading to substorm onset, *J. Geophys. Res., 108(A3)*, 1119, doi:10.1029/2002JA009670, 2003.

Nagel, S. R., Instabilities in a sandpile, *Rev. Mod. Phys., 64*, 321, 1992.

Ohtani, S., T. Higuchi, A. T. Y. Lui, and K. Takahashi. Magnetic fluctuations associated with tail current disruption: Fractal analysis, *J. Geophys. Res., 100*, 19,135, 1995.

Osborne, A. R. and A. Provenzale, Finite correlation dimensions for stochastic systems with power-law spectra, *Physica D, 35*, 357, 1989.

Packard, N., J. Crutchfield, D. Farmer, and R. Shaw, Geometry from a time series, *Phys. Rev. Lett., 45*, 712, 1980.

Pavlos, G. P., G. A. Kyriakov, A. G. Rigas, P. I. Liatsis, P. C. Trochoutsos, and A. A. Tsonis, Evidence for strange attractor structures in space plasmas, *Ann. Geophys., 10*, 309, 1992.

Pavlos, G. P., D. Diamandidis, A. Adamopoulos, A. G. Rigas, I. A. Daglis, and E. T. Sarris, Chaos and magnetospheric dynamics, *Nonlin. Proc. Geophys., 1*, 124, 1994.

Pavlos, G. P., M. A. Athanasiu, D. Diamandidis, A. G. Rigas, and E. T. Sarris, Comments and new results about the magnetospheric chaos hypothesis, *Nonlin. Proc. Geophys., 6*, 99, 1999.

Preisendorfer, R. W., *Principal Component Analysis in Meteorology and Oceanography*, Elsevier, New York, 1988.

Press, W. H., B. P. Flannery, S. A. Teukolsky, and W. V. Vetterling, *Numerical Recipes: The Arth of Scientific Computing*, 2nd ed., Cambridge Univ. Press, New York, 1992.

Price, C. P., and D. Prichard, The chaotic or non-chaotic behabior of global geomagnetic processes, in: *Physics of Space Plasmas*, SPI Conf. Proc. And Reprint Ser., No.12, Scientific Publ., Inc., Cambridge, MA, pp.265-277, 1992.

Prichard, D., Comment on "Chaos and magnetospheric dynamics" by G. P. Pavlos, D. Diamandidis, A. Adamopoulos, A. G. Rigas, I. A. Daglis, and E. T. Sarris, *Nonlin. Proc Geophys., 2*, 58, 1995.

Prichard, D., and C. P. Price, Spurious dimension estimates from time series of geomagnetic indices, *Geophys. Res. Lett., 19*, 1623, 1992.

Prichard, D., J. E. Borovsky , P. M. Lemons, C. P. Price, Time dependence of substorm recurrence: An information-theoretic analysis, *J. Geophys. Res., 101*, 15,359, 1996.

Roberts, D. A., Is there a strange attractor in the magnetosphere?, *J. Geophys. Res., 96*, 16,031, 1991.

Shan, L. H., P. Hansen, C. K. Goertz, and R. A. Smith, Chaotic appearance of the ae index, *Geophys. Res. Lett., 18*, 147, 1991a.

Shan, L. H., C. K. Goertz, and R. A. Smith, On the embedding-dimension analysis of ae and al time series, *Geophys. Res. Lett., 18*, 1647, 1991b.

Sharma, A. S., assessing the magnetosphere's nonlinear behavior: Its dimension is low, its predictability, high, *Rev. Geophys. Suppl.*, pp.645-650, 1995.

Sharma, A. S., D. V. Vassiliadis, and K. Papadopoulos, Reconstruction of low-dimensional magnetospheric dynamics by singular spectrum analysis, *Geophys. Res. Lett., 20*, 335, 1993.

Sitnov, M. I., H. V. Malova, and A. T. Y. Lui, Quasi-neutral sheet tearing instability induced by electron preferential acceleration from stochasticity, *J. Geophys. Res., 102*, 163, 1997.

Sitnov, M. I., A. S. Sharma, K. Papadopoulos, D. Vassiliadis, J. A. Valdivia, A. J. Klimas and D. N. Baker, Phase transition-like behavior of the magnetosphere during substorms, *J. Geophys. Res., 105*, 12,955, 2000.

Sitnov, M. I., A. S. Sharma, K. Papadopoulos, and D. Vassiliadis, Modeling substorm dynamics of the magnetosphere: From self-organization and self-organized criticality to nonequilibrium phase transitions, *Phys. Rev. E, 65*, 016116, 2001.

Smith, A. J., M. P. Freeman, and G. D. Reeves, Postmidnight VLF chorus events, a substorm signature observed at the ground near $L = 4$, *J. Geophys. Res., 101*, 24,641, 1996

Stanley, H. E., *Introduction to Phase Transition and Critical Phenomena*, Oxford Univ. Press, New York, 1971.

H.E. Stanley, Scaling, universality, renormalization: three pillars of modern critical phenomena, *Rev. Mod. Phys. 71*, S358, 1999.

Tabor, M., *Chaos and Integrability in Nonlinear Dynamics*, John Wiley & Sons, 1989.

Takalo, J., J. Timmonen, A. Klimas, J. Valdivia, and D. Vassiliadis, Nonlinear energy dissipation in a cellular automation magnetic field model, *Geophys. Res. Lett., 26,* 1813, 1999.

Takalo, J., J. Timmonen, A. Klimas, J. Valdivia, and D. Vassiliadis, A coupled-map model for the magnetotail current sheet, *Geophys. Res. Lett., 26,* 2913, 1999.

Takens, Detecting strange attractors in turbulence, in: *Lecture Notes in Mathematics 898,* D. A. Rand and L. S. Young, eds., Springer, Berlin, pp. 366-381, 1981.

Theiler, J., Spurious dimension from correlation algorithms applied to limited time series data, *Phys. Rev. A, 34,* 2427, 1986.

Theiler, J., Some comments on the correlation dimension of $1/f^{\alpha}$ noise, *Phys. Lett. A, 155,* 480, 1991.

Tsurutani, B. T., M. Sugiura, T. Iyemori, B. E. Goldstein, W. D. Gonzalez, S. I. Akasofu, and E. J. Smith, The nonlinear response of AE to the IMF Bs driver: A spectral break at 5 hours, *Geophys. Res. Lett., 17,* 279, 1990.

Ukhorskiy, A. Y., M. I. Sitnov, A. S. Sharma, and K. Papadopoulos, Global and multi-scale aspects of magnetospheric dynamics in local-linear filters, *J. Geophys. Res., 107*(A11), 1369, doi: 10.1029/2001JA009160, 2002.

Ukhorskiy, A. Y., M. I. Sitnov, A. S. Sharma, and K. Papadopoulos, Global and multi-scale features in a description of the solar wind-magnetosphere coupling, *Ann. Geophys., 21,* 1913, 2003.

Ukhorskiy, A. Y., M. I. Sitnov, A. S. Sharma, and K. Papadopoulos, Combining global and multi-scale features of the solar wind-magnetosphere coupling: From modeling to forecasting, *Geophys. Res. Lett., 31,* L08802, doi:10.1029/2004GL018932, 2004a.

Ukhorskiy, A. Y., M. I. Sitnov, A. S. Sharma, B. J. Anderson, S. Ohtani, and A. T. Y. Lui, Data-derived forecasting model for relativistic electron intensity at geosynchronous orbit, *Geophys. Res. Lett., 31,* L09806, doi:10.1029/2004GL019616, 2004b.

Uritsky, V. M., and M. I. Pudovkin, Low frequency 1/f-like fluctuations of the AE index as a possible manifestation of self-organized criticality in the magnetosphere, *Ann. Geophys., 16(12),* 1580, 1998.

Uritsky, V. M., A. J. Klimas, and D. Vassiliadis, Multiscale dynamics and robust critical scaling in a continuum current sheet model, *Phys. Rev. E, 65,* 046113, 2002.

Uritsky, V. M., A. J. Klimas, D. Vassiliadis, D. Chua, G. Parks, Scale-free statistics of spatiotemporal auroral emissions as depicted by POLAR UVI images: Dynamic magnetosphere is an avalanching system, *J. Geophys. Res., 107(A12),* 1426, doi:10.1029/1001JA000281, 2002.

Valdivia, J. A., A. S. Sharma, and K. Papadopoulos, Prediction of magnetic storms by nonlinear models, *Geophys. Res. Lett., 23,* 2899, 1996.

Vassiliadis, D., A. S. Sharma, T. E. Eastman, and K. Papadopoulos, Low-dimensional chaos in magnetospheric activity from AE time series, *Geophys. Res. Lett., 17,* 1841, 1990.

Vassiliadis, D., A. J. Klimas, D. Baker, and D. A. Roberts, A description of the solar wind-magnetosphere coupling based on nonlinear filters, *J. Geophys. Res., 100,* 3495, 1995.

Vespignani, A., and S. Zapperi, How self-organized criticality works: A unified mean-field picture, *Phys. Rev. E, 57,* 6345, 1998.

Watkins, N. W., S. C. Chapman, R. O. Dendy, and G. Rowlands, Robustness of collective behaviour in strongly driven avalanche models: Magnetospheric implications, *Geophys. Res. Lett., 26,* 2617, 1999.

Watkins, N. W., M. P. Freeman, S. C. Chapman, and R. O. Dendy, Testing the SOC hypothesis for the magnetosphere, *J. Atm. Sol. Terr. Phys., 63,* 1435, 2001.

Weigel, R.S., W. Horton, T. Tajima, and T. Detman, Forecasting auroral electrojet activity from solar wind input with neural networks, *Geophys. Res. Lett., 26,* 1353, 1999.

Weigel, R.S., A.J. Klimas, D. Vassiliadis, V. Uritsky, and W. Horton, Features of auroral zone magnetometer time series during undriven relaxation, Spring AGU meeting, Boston, MA, May 29-June 2, Abstract SM61B-06, 2001.

Zheng, G. P., and J. X. Zhang, Determination of dynamical critical exponents from hysteresis scaling, *Phys. Rev. E, 58*, 1187, 1998.